npj | climate and atmospheric science

www.nature.com/npjclimatsci

ARTICLE OPEN

Check for updates

Atmospheric NO_x oxidation as major sources for nitrous acid (HONO)

Min Song[1,2,7], Xiaoxi Zhao[1,3,4,7], Pengfei Liu[1,4,7]✉, Jichun Mu[1,4,5], Guangzhi He[1,4], Chenglong Zhang[1,4], Shengrui Tong[4,6], Chaoyang Xue[1], Xiujuan Zhao[3], Maofa Ge[4,6] and Yujing Mu[1,4]✉

Nitrous acid (HONO) is the major precursor of hydroxyl (OH) radicals to initiate tropospheric chemistry leading to formation of secondary pollutants. The sources of atmospheric HONO, however, are not fully understood. Here we show two additional HONO sources that stem from atmospheric oxidation of nitrogen oxide ($NO_x = NO + NO_2$). Nitric acid (HNO_3) formed from photooxidation of NO_2 can be converted into HONO with a yield of ~53%, and dark NO oxidation by NO_3 radicals in the presence of H_2O produces HONO with a yield of 2%. The diurnal variations of HONO levels from field observations in the urban (Beijing) and rural (Wangdu) areas of the North China Plain can be well reproduced by the WRF-Chem model when the two new HONO sources are taken into account. The findings imply that atmospheric NO_x oxidation pathways are the major sources for HONO, which can significantly accelerate ozone formation in polluted regions as well.

npj Climate and Atmospheric Science (2023)6:30 ; https://doi.org/10.1038/s41612-023-00357-8

INTRODUCTION

Atmospheric nitrous acid (HONO) can be quickly photolyzed to produce hydroxyl (OH) radicals under weak sunlight irradiation in the early morning, and thus it has long been recognized as the initiator for triggering daytime atmospheric chemistry in the lower atmosphere[1]. A large number of studies further reveal that daytime HONO over polluted areas also acts as the major or even dominant source for OH radicals, accounting for 20–90% of the total OH primary production[2,3]. However, the sources of HONO were not fully understood, e.g., there exist a large missing HONO source in daytime based on the field measurements[4–6]. To explain the missing source of daytime HONO, several potential HONO sources have been proposed, including the photo-enhanced reduction of NO_2 by organic materials[7–9], the photolysis of adsorbed nitric acid (HNO_3) or particulate nitrate[10–13], soil emission through biogenic production[14,15], displacement of strong acids on soil surface[16,17], the reaction of excited gaseous NO_2 with water[18,19], the photolysis of nitrophenols[20,21], and the reaction of HO_2·H_2O complexes with NO_2[22]. Among the proposed HONO sources, the photo-enhanced reduction of NO_2 by organic materials on ground surface is commonly considered as the dominant HONO source in daytime[2,23]. Nevertheless, there are still large gaps in daytime HONO levels between the observations and model simulations after the proposed HONO sources are taken into consideration[4,24,25].

Considering that NO_x (NO and NO_2) is the predominant precursor for HONO formation[26,27], the unknown HONO sources might be related to some additional NO_x reactions. Therefore, it is necessary to further investigate the possible HONO formation from the atmospheric oxidation of NO_x. In this study, a series of experiments were conducted in a smog chamber to reveal the possible HONO formation channels from photo- and dark-oxidation of NO_x. Finally, the contributions of the potentially proposed mechanisms to atmospheric HONO and O_3 were also assessed by the Weather Research and Forecasting coupled with chemistry (WRF-Chem) model.

RESULTS AND DISCUSSION

HONO formation from photooxidation of NOx

The variations of HONO and the key species (NO, NO_2 and O_3) in six gas mixtures of NO_x under both dark and light conditions are illustrated in Fig. 1 and Supplementary Fig. 1, respectively. Before the irradiation, HONO concentration in each mixture was relatively stable within the one-hour duration (Fig. 1), implying the heterogeneous reactions of NO_x on the inherent chamber wall made ignorable contribution to HONO production. The relatively high initial HONO concentrations (0.7–1.7 ppb) in the chamber were mainly ascribed to HONO formation from heterogeneous reactions of the standard gases (NO_2 and NO) in the cylinders, e.g., HONO concentration in the chamber could be reduced by 85.6% when the same amount of NO_2 standard gas was introduced into the chamber through a tube filled with and without particulate sodium hydrate. In contrast to the relatively stable HONO concentration before the irradiation, HONO levels displayed evidently increasing trends after stopping the irradiation (Fig. 1), indicating that the photochemical products formed during the irradiation were involved in the dark HONO formation. During the irradiation, HONO levels in all the mixtures initially displayed quickly decreasing trends due to HONO photolysis. Subsequently, HONO levels became relatively stable in the mixtures of NO_x + air and $NO_2 + O_2$, whereas they exhibited remarkably increasing trend in the mixture of $NO_2 + N_2$ after a period of irradiation (Fig. 1a). Additionally, there was significant difference in HONO levels between the two air mixtures of 300 ppb NO_2 + 200 ppb NO with

[1]Research Center for Eco-Environmental Sciences, Chinese Academy of Sciences, Beijing 100085, China. [2]School of Environmental Science and Engineering, Shandong University, Qingdao 266237, China. [3]Institute of Urban Meteorology, Chinese Meteorological Administration, Beijing 100089, China. [4]University of Chinese Academy of Sciences, Beijing 100049, China. [5]State Key Laboratory of Environmental Aquatic Chemistry, Research Center for Eco-Environmental Sciences, Chinese Academy of Sciences, Beijing 100085, China. [6]State Key Laboratory for Structural Chemistry of Unstable and Stable Species, CAS Research/Education Center for Excellence in Molecular Sciences, Institute of Chemistry, Chinese Academy of Sciences, Beijing 100190, PR China. [7]These authors contributed equally: Min Song, Xiaoxi Zhao, Pengfei Liu.
✉email: pfliu@rcees.ac.cn; yjmu@rcees.ac.cn

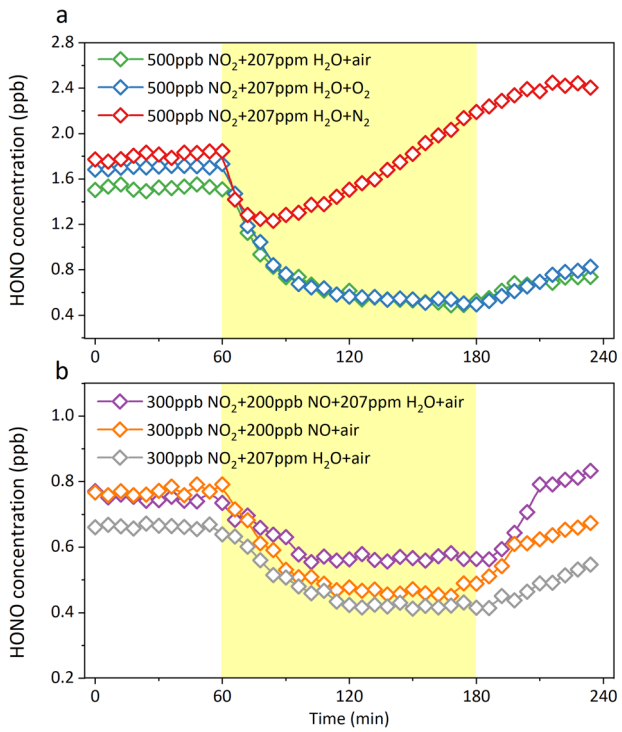

Fig. 1 The variations of HONO concentration among the six mixtures under both dark and light conditions in the smog chamber. a 500 ppb NO_2 + 207 ppm H_2O + air/O_2/N_2, **b** 300 ppb NO_2 + 200 ppb NO +207 ppm H_2O + air, 300 ppb NO_2 + 200 ppb NO + air, 300 ppb NO_2 + 207 ppm H_2O + air. The yellow shadows represent the UV-light irradiation.

and without the existence of H_2O during the irradiation although their initial HONO concentrations were almost identical (Fig. 1b).

To explore the reasons for the distinct difference in HONO variations among the irradiated mixtures, HONO loss and formation rates in each mixture were analyzed based on the key reactions (Eqs. 1–3) that are often considered as the basis for judging the daytime unknown HONO sources in many areas[6]. J_{HONO} was calculated to be about $1.0 \times 10^{-3}\,s^{-1}$ according to the first-order decay law of HONO in the chamber (See Supplementary Methods and Supplementary Fig. 2), and the levels of OH radicals were estimated based on the assumption that OH radicals in the irradiated mixtures were in a steady state through Eqs. 1–4[28,29] (See Supplementary Methods and Supplementary Fig. 3).

$$HONO + h\nu \rightarrow OH + NO \quad J_{HONO} \tag{1}$$

$$NO + OH \rightarrow HONO \quad k_2 = 3.3\times10^{-11}\,cm^3\,molecule^{-1}s^{-1} \tag{2}$$

$$HONO + OH \rightarrow NO_2 + H_2O \quad k_3 = 6.0\times10^{-12}\,cm^3\,molecule^{-1}s^{-1} \tag{3}$$

$$NO_2 + OH \rightarrow HNO_3 \quad k_4 = 2.6\times10^{-11}\,cm^3\,molecule^{-1}s^{-1} \tag{4}$$

As shown in Fig. 2, HONO loss rates via Eqs. 1 and 3 were evidently faster than its formation rate through Eq. 2 in all the mixtures during the irradiation. Obviously, besides Eq. 2, there existed unknown HONO sources to account for the nondecreasing HONO levels in the mixtures of NO_x + air, $NO_2 + O_2$ and $NO_2 + N_2$ during the irradiation (Fig. 1a). The unknown HONO formation rates were calculated according to the following equation (Eq. 5), which showed distinct differences among the irradiated mixtures (Fig. 2).

$$HONO_{unknown} = HONO_{loss} - HONO_{formation} - \frac{d[HONO]_{meas}}{dt} \tag{5}$$

Additionally, the higher ratio of NO to NO_2 during the irradiation (Supplementary Fig. 1) significantly increased HONO formation through the reaction of NO with OH radicals, but evidently suppressed the unknown HONO formation rates (Fig. 2).

As the smog chamber is made of inert Teflon film without conducting any experiments in the presence of organic compounds, the photo-enhanced reduction of NO_2 by organic materials[7–9] could be excluded for the unknown HONO sources in the irradiated mixtures. Although the heterogeneous NO_2 conversion on the Teflon surface in the presence of H_2O could also contribute to HONO[30,31], its reaction rate was too slow to explain the unknown HONO sources due to no photo-enhancement in the kinetics of the reaction[32,33]. The possible HONO formation through reaction of $HO_2{\cdot}H_2O$ complexes with NO_2[22] could be also excluded because HO_2 formation rates through reaction of OH with O_3 (See Supplementary Methods and Supplementary Fig. 4) were at least 2 orders of magnitude slower than the unknown HONO formation rates in the irradiated mixtures (Fig. 2). The quantum yield for ground state oxygen atom (O^3P) and NO from photolysis of NO_2 is unity under <400 nm ultraviolet irradiation[34], and thus HONO formation through the reaction of excited NO_2 with water[18,19] might be negligible in the irradiated mixtures because the black-light lamps used for the irradiation mainly emit 330–400 nm ultraviolet with the central wavelength of 365 nm (Supplementary Fig. 5). Considering the evident increase of HNO_3 levels formed through Eq. 4 in the mixtures of NO_x during the irradiation (Supplementary Fig. 6), the unknown HONO formation in the irradiated mixtures was suspected to be related to the reactions involving in HNO_3. The above speculation could be supported by the significantly linear correlation ($R^2 = 0.99$) between the average unknown HONO formation rates and the HNO_3 formation rates for the five mixtures with the same H_2O concentration (~207 ppm) (Fig. 3). It should be noted that the data point for the mixture of NO_2 + NO without the existence of H_2O was found to evidently deviate from the linear correlation (Fig. 3), implying that H_2O is also involved in HONO formation through the reactions associated with HNO_3. In addition, less HNO_3 formation could be expected for the irradiated mixtures with increasing the NO/NO_2 ratio (Supplementary Fig. 1) due to the competition reactions of NO and NO_2 with OH radicals, resulting in evident decrease of the unknown HONO formation rates (Fig. 2).

Based on the above photooxidation experiments in the presence of H_2O, the unknown HONO formation rate (ppb s^{-1}) associated with HNO_3 formation rate (ppb s^{-1}) (Fig. 3) could be overall expressed as:

$$\frac{d[HONO]}{dt} = 0.53\times\frac{d[HNO_3]}{dt} + 1.2\times10^{-4}\,(ppb\,s^{-1}) \tag{6}$$

It should be noted that the interception of 1.2×10^{-4} in Fig. 3 was the average unknown HONO formation rate (ppb s^{-1}) when the average HNO_3 formation rate was zero, indicating that there still existed the unknown HONO sources other than the reactions related to HNO_3, e.g., the potential contribution from the gas-phase reaction of NO with OH radicals produced from blank Teflon chambers under ultraviolet irradiation[35] to HONO.

Although photolysis of adsorbed HNO_3 (HNO_3(ad)) (Eq. 7) has been proposed to be an important source for atmospheric HONO, it might be negligible in the irradiated mixtures because it usually occurs under the irradiation with wavelengths less than 320 nm[11]. Considering the relatively fast increase of HONO levels for the irradiated mixtures with relatively high NO concentrations just after turning off the UV lamps (Fig. 1), the possible reaction of NO

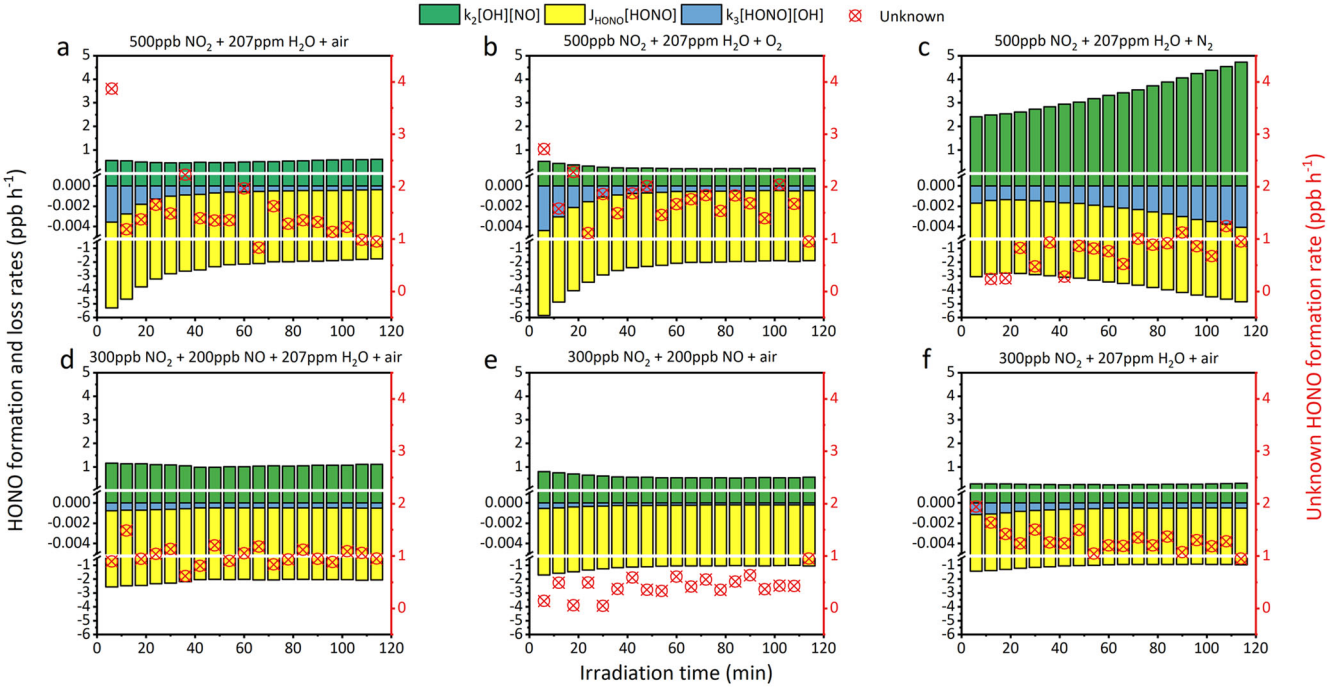

Fig. 2 The formation and loss rates of HONO in the six mixtures of NO_x during the irradiation periods. a 500 ppb NO_2 + 207 ppm H_2O +air, **b** 500 ppb NO_2 + 207 ppm H_2O + O_2, **c** 500 ppb NO_2 + 207 ppm H_2O + N_2, **d** 300 ppb NO_2 + 200 ppb NO + 207 ppm H_2O + air, **e** 300 ppb NO_2 + 200 ppb NO + air, **f** 300 ppb NO_2 +207 ppm H_2O + air. Formation rate: k_2[OH][NO] is the HONO formation rate through gas-phase reaction of NO with OH radicals (Eq. 2); loss rates: J_{HONO}[HONO] is the photolysis rate of HONO (Eq. 1) and k_3 [HONO][OH] is the HONO consumption rate by reaction with OH radicals (Eq. 3).

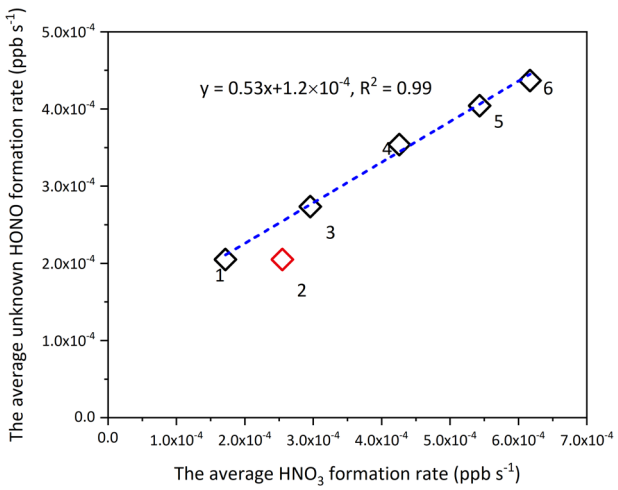

Fig. 3 The correlation between the average unknown HONO and HNO_3 formation rates. Note that: 1. 500 ppb NO_2 + 207 ppm H_2O + N_2; 2. 300 ppb NO_2 + 200 ppb NO + air; 3. 300 ppb NO_2 + 200 ppb NO + 207 ppm H_2O + air; 4. 300 ppb NO_2 + 207 ppm H_2O + air; 5. 500 ppb NO_2 + 207 ppm H_2O + air; 6. 500 ppb NO_2 + 207 ppm H_2O + O_2.

with HNO_3 was suspected to contribute to HONO formation. Therefore, the possible HONO formation from the reaction of NO with HNO_3(ad) was further investigated in the chamber by using long path absorption photometer (LOPAP) for HONO measurement under dark condition. As shown in Fig. 4a, b, the HONO concentration quickly increased from zero to about 50 ppt after adding 100 ppb NO into the chamber containing the purified air, whereas HONO concentration kept zero when the same amount of NO was introduced into the chamber containing the air mixture in the presence of 6 ppm HNO_3 and 200 ppm H_2O. The high HNO_3 concentration could greatly reduce HONO absorption efficiency in the stripping coil of the LOPAP due to decrease of pH in the absorption solution, which might mask the possible HONO formation in the chamber. As expected, HONO concentration sharply increased from zero to more than 3 ppb when the same amount of NO was introduced into the chamber that has been exposed to 6 ppm HNO_3 and 200 ppm H_2O for one week and then cleaned with the purified air for four times (Fig. 4c, the green data points). The HONO concentration could still increase from zero to ~500 ppt for the second introduction of NO after the chamber being cleaned again (Fig. 4c, the blue data points), which was at least a factor of 5 higher than that of the chamber experiment with NO addition before introducing HNO_3 (Fig. 4a). Because the gas phase reaction of NO with HNO_3 is extremely slow[36] and a certain amount of HNO_3 might be absorbed on the chamber wall after the exposure of the high HNO_3 concentration due to its viscosity, the HONO formation might be from the heterogeneous reaction of NO with HNO_3(ad) (Eq. 8) on the chamber wall.

$$HNO_{3(ad)} + h\nu\,(\lambda < 320nm) \rightarrow HONO \quad (7)$$

$$NO + HNO_{3(ad)} \overset{Surface}{\rightarrow} HONO + NO_2 \quad (8)$$

Based on the quick increase of HONO concentration just after addition of NO for the chamber experiments, the heterogeneous reaction of NO with HNO_3(ad) might be very fast. The HNO_3(ad) on the chamber wall might be in multiple layers and only the HNO_3(ad) at the uppermost layer could be involved in HONO formation, resulting in the stable HONO level after its pulse increase owing to the quick termination of the heterogeneous reaction with depleting the HNO_3(ad) at the uppermost layer. The HNO_3(ad) at the inner layers could be exposed again to the surface layer after cleaning the chamber by the purified air,

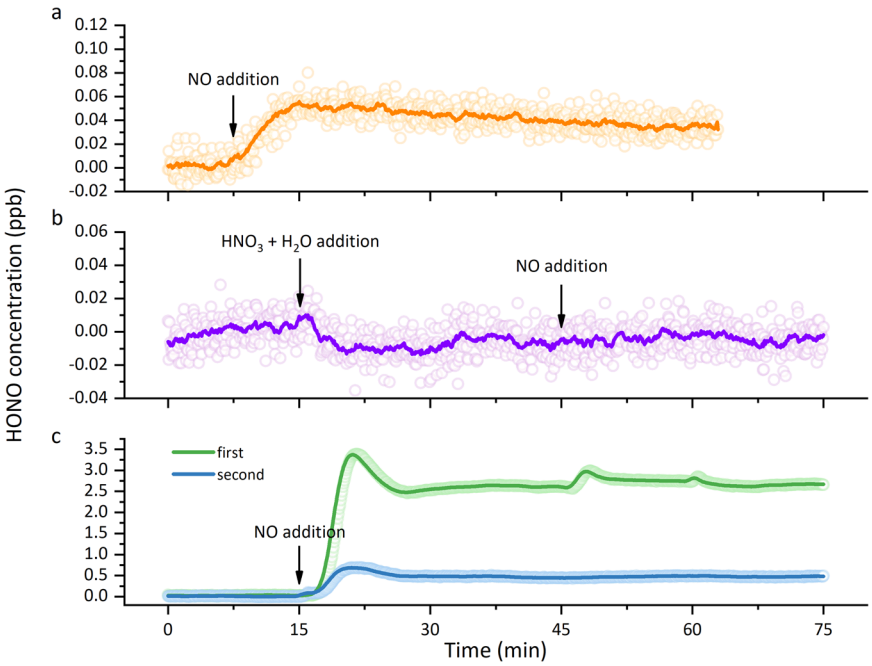

Fig. 4 The variations of HONO concentration for the mixtures of NO and HNO_3 under dark condition in the smog chamber. a 100 ppb NO + air, **b** 6 ppm HNO_3 + 200 ppm H_2O + 100 ppb NO + air; **c** <6 ppm HNO_3(ad) + <200 ppm H_2O + 200 ppb NO + air. The black arrows indicate the time for introducing the reactants into the chamber.

explaining the significant increase of HONO level for the second experiment with NO addition. As for the irradiated gas mixtures of NO_x, the continuous HNO_3 formation through the photochemical reaction of NO_2 with OH could guarantee that the fresh HNO_3(ad) on the wall surface was always exposed to NO, resulting in the high HONO yield (~53%) from the HNO_3 conversion through the heterogeneous reaction (Eq. 8).

HONO formation through the heterogeneous reaction of NO with HNO_3(ad) on particles has also been proposed to account for significant overestimation of [HNO_3]/[NO_x] ratio by photochemical models in comparison with measurements performed in the free troposphere[37] and over the boundary layer of polluted urban atmospheres[38]. Quick increase of HONO levels was also observed after exposing NO to the HNO_3(ad) on soot by a previous study in a low-pressure flow reactor (Knudsen cell)[39]. Based on a small quantity of HNO_3(ad) consumption in the presence of NO, the heterogeneous reaction (Eq. 8) was considered as a slow reaction by the above study[39]. However, the heterogeneous reaction rate might be largely underestimated because of the multiple layers of HNO_3(ad) on the soot.

HONO formation from dark-oxidation of NO_x

The dark-oxidation of NO_x by O_3 can also produce HNO_3 through Eqs. 9–12[29], and thus HONO formation is also expected to occur during the dark-oxidation process. To verify the conjecture, a series of chamber experiments under dark condition were conducted by continuously introducing the NO standard gas (403 ppm in N_2) at a fixed flow rate of 20 mL min^{-1} (2.7 ppb min^{-1} equally) into air mixtures with different initial O_3 concentrations (0, ~100, ~220, and ~280 ppb). As shown in Fig. 5a, HONO levels were almost identical in the air mixtures with initial O_3 concentrations of 0 ppb and ~100 ppb during the entire period, whereas they significantly increased in the air mixtures with initial O_3 concentrations of ~220 ppb and ~280 ppb after introducing NO.

$$O_3 + NO \rightarrow NO_2 + O_2 \quad k_6 = 1.8\times 10^{-14}\text{cm}^3\,\text{molecule}^{-1}\text{s}^{-1} \tag{9}$$

$$O_3 + NO_2 \rightarrow NO_3 + O_2 \quad k_7 = 3.5\times 10^{-17}\text{cm}^3\,\text{molecule}^{-1}\text{s}^{-1} \tag{10}$$

$$NO_3 + NO_2 \rightarrow N_2O_5 \quad k_8 = 1.9\times 10^{-12}\text{cm}^3\,\text{molecule}^{-1}\text{s}^{-1} \tag{11}$$

$$N_2O_5 + H_2O_{(ad)} \rightarrow HNO_3 \tag{12}$$

$$N_2O_5 \rightarrow NO_3 + NO_2 \quad k_9 = 0.07\text{s}^{-1} \tag{13}$$

$$NO_3 + NO \xrightarrow{M(N_2,O_2)} NO_2 \quad k_{10} = 2.6\times 10^{-11}\text{cm}^3\,\text{molecule}^{-1}\text{s}^{-1} \tag{14}$$

Although dark reactions (Eqs. 9–14) can occur in all the air mixtures, the reaction extent largely depends on the initial O_3 concentrations. For the air mixture with initial O_3 concentration of ~100 ppb, O_3 was mainly consumed by reaction with NO (Eq. 9), which suppressed NO_3 formation from the reaction of O_3 with NO_2 (Supplementary Figs. 7 and 8), resulting in negligible N_2O_5 accumulation (Fig. 5b). As for the air mixtures with higher initial O_3 concentrations, the reaction of O_3 with NO_2 (Eq. 10) was significantly accelerated because of their relatively high concentrations during introduction of NO (Supplementary Fig. 7c and d), leading to remarkable formation of NO_3 (Supplementary Fig. 8) and evident accumulation of N_2O_5 (Fig. 5b). The quick decrease of N_2O_5 levels after their peak values in the two mixtures with high initial O_3 concentrations were attributed to the reaction of NO with NO_3 which suppressed N_2O_5 formation rate through Eq. 11 and accelerated N_2O_5 consumption rate through Eq. 13. More HNO_3 could be formed with increasing N_2O_5 levels in the chamber because of the heterogeneous reaction of N_2O_5 with the absorbed H_2O on the chamber wall (Eq. 12). The evidently faster increase of HONO levels with increasing the initial O_3 concentrations (Fig. 5a) further indicated that HONO formation was possibly associated

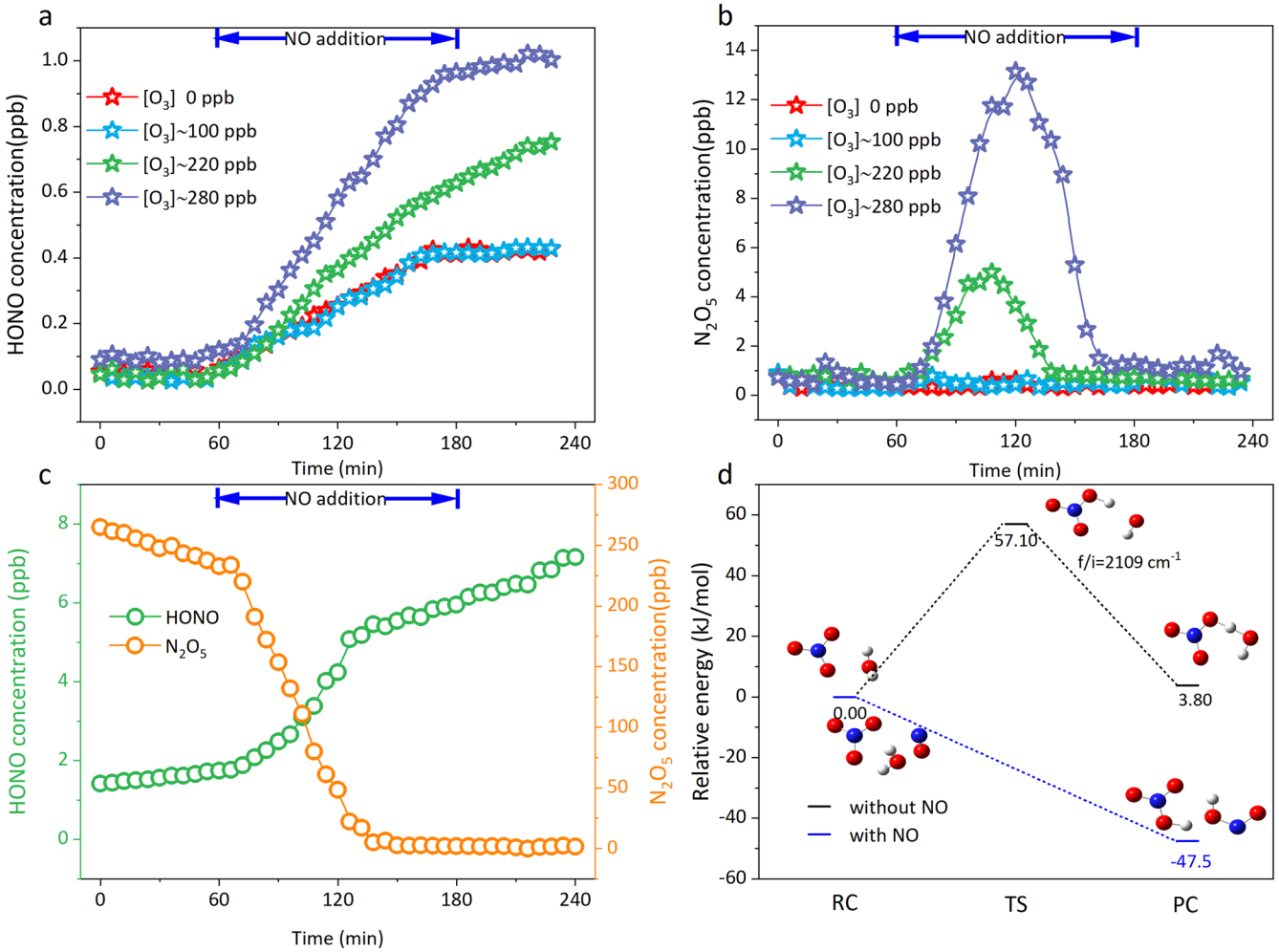

Fig. 5 HONO formation from the reaction of NO_3 with NO under the dark condition. a, **b** The HONO and N_2O_5 concentrations for the mixtures with different initial O_3 concentrations and ~207 ppm H_2O, respectively; **c** the HONO and N_2O_5 concentrations for the mixture with the initial ~260 ppb N_2O_5 concentration and ~828 ppm H_2O (See Supplementary Methods); note that the NO standard gas was added continuously into the chamber with the flow rate of 20 mL/min from 60 to 180 min for (**a**), (**b**) and (**c**); **d** pathways for the reaction of NO_3 with H_2O to produce HONO with and without the existence of NO as well as the optimized geometries of the reactant complex (RC), transition state (TS) and product complex (PC). Blue, red and white circles represent N, O and H atoms, respectively.

with the forementioned heterogeneous reaction involving in HNO_3. Compared with the period after depletion of N_2O_5, the increase of HONO level was evidently faster during the period when obvious N_2O_5 was present (Fig. 5a, b), implying that other reactions besides Eq. 8 might also make contribution to HONO formation.

The reaction of NO_3 with NO was suspected to produce HONO because NO_3 concentration was relatively high during the period in the presence of N_2O_5 (Supplementary Fig. 7). To certify the suspicion, dark experiments were further conducted by introducing NO into air mixtures of N_2O_5 (See Supplementary Methods). The variations of HONO and N_2O_5 levels in the air mixture are shown in Fig. 5c and those of NO, NO_2 and O_3 concentrations are illustrated in Supplementary Fig. 9. As shown in Fig. 5c, after introducing NO into the chamber, the abrupt increase of HONO level was well accompanied with quick decrease of N_2O_5 concentration. Additionally, the increase of HONO level displayed a turning point when N_2O_5 concentration approached zero. Due to small O_3 concentration in the air mixture of N_2O_5 before introducing NO (Supplementary Fig. 9), the introduced NO mainly reacted with NO_3 leading to fast decrease of N_2O_5 and quick increase of NO_2 through Eqs. 13–14. Based on the significantly linear correlation ($R^2 = 0.997$) between the increment of HONO and the decrease of N_2O_5 with the slope of 0.02 (Supplementary Fig. 10), HONO yield of ~2% could be obtained due to NO_3 consumption.

To account for the above phenomenon, the reaction (Eq. 15) was proposed.

$$NO_3 + NO + H_2O \rightarrow HNO_3 + HONO \quad (15)$$

The proposed reaction (Eq. 15) was verified to be feasible through Density Functional Theory (DFT) calculations (See Supplementary Methods), which is barrierless in comparison with the extremely higher energy barrier for the reaction of NO_3 with H_2O (Fig. 5d).

Atmospheric implication

Atmospheric NO_x could also experience the same oxidation processes as the cases of the simulation in the chamber, and hence the unknown HONO sources identified through the chamber experiments are also expected to occur in the real atmosphere. To assess the contribution of atmospheric NO_x oxidation to HONO, atmospheric HONO levels at two sampling sites of a rural area (Station of Rural Environment, Research Center for Eco-Environmental Sciences, SRE-RCEES[40–42]) and Beijing city

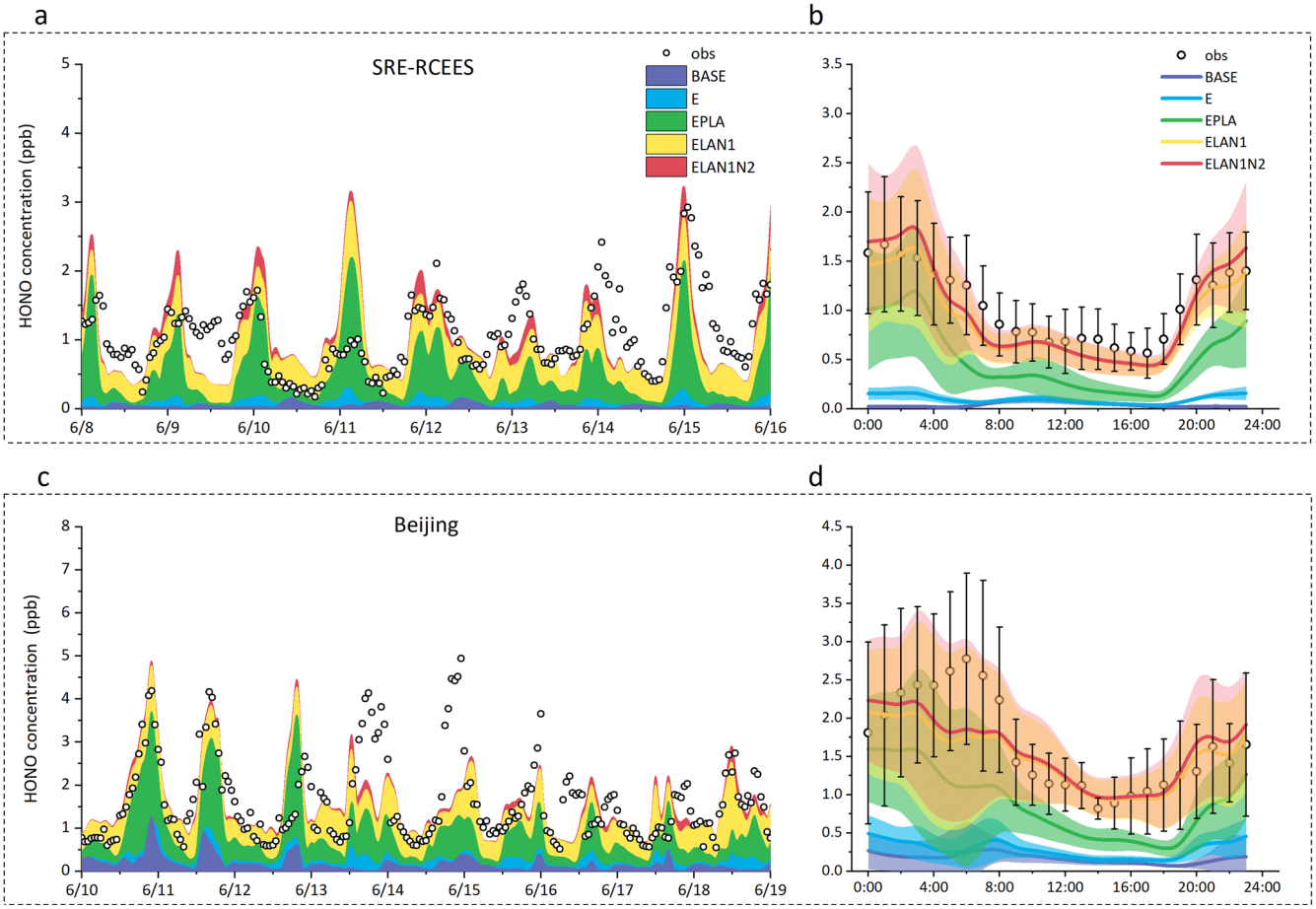

Fig. 6 Time series and average diurnal variation of simulated HONO from different scenarios versus the observed HONO at SRE-RCEES and IAP of the NCP. a, **b** Time series and average diurnal variation of simulated and observed HONO at SRE-RCEES, respectively; **c**, **d** time series and average diurnal variation of simulated and observed HONO at IAP, respectively. The different scenarios contain BASE, E, EPLA, ELAN1 and ELAN1N2 (see Supplementary Methods and Supplementary Table 1).

(Institute of Atmospheric Physics, IAP[43]) in the NCP were simulated by the WRF-Chem model with incorporation of the two HONO formation pathways identified in this study (See Supplementary Methods).

For the scenarios BASE (only considering the gas-phase HONO formation) and E (BASE plus direct HONO emissions), the simulated HONO levels were about one order of magnitude lower than the observed values (Fig. 6), which was in agreement with previous modeling results[44,45]. The simulation was significantly improved after further considering the major highlighted HONO sources for the scenario EPLA (E plus the photolysis of particulate nitrate, and the (photo-enhanced) heterogeneous reactions of NO_2 on land and aerosol surfaces), but the simulated daytime HONO levels were only about half of the observed values. The scenario ELAN1 (E plus the heterogeneous reactions of NO_2 on land and aerosol surfaces, and the NO_x photooxidation in daytime) could well reproduce the daytime HONO levels even if the photo-enhanced heterogeneous reactions of NO_2 and the photolysis of particulate nitrate were not taken into consideration, implying the significant role of the NO_x photooxidation in HONO formation over the polluted areas. Additionally, the HONO formation from the reaction of NO_3 with NO also made great contribution to nighttime HONO, as shown in Fig. 6 for the scenario ELAN1N2 (ELAN1 plus NO oxidation by NO_3 in nighttime).

Many field studies reported that the daytime missing HONO sources showed significant correlations with the product of NO_2 photolysis rate coefficient (J_{NO2}) and NO_2 concentration (C_{NO2}), and thus photo-enhanced reductions of NO_2 on the surfaces of aerosols and ground were proposed to be the major source of daytime HONO[6,46]. As the diurnal variation of J_{NO2} is in line with OH concentration (C_{OH}) at ground level[47], the daytime missing HONO sources could also be expected to significantly correlate with the product of $k_4 \times C_{OH} \times C_{NO2}$, namely HNO_3 formation rates. The photo-enhanced conversion of NO_2 to HONO identified in the flow tube experiments[7,8] might also be partially viewed as the contribution from the forementioned heterogeneous reaction associated with HNO_3 because HNO_3 could be formed through reactions of NO_x with HO_x ($OH + HO_2$) radicals that are recently found to be produced by irradiating atmospheric particles[48,49] and organic mixtures[50].

Compared with the scenario BASE, the simulated O_3 levels by the scenario ELAN1N2 had noticeable enhancements (~38.4%) and were in good agreement with the observations at multiple monitoring stations across the NCP (Supplementary Fig. 11), implying the additional HONO sources over the NCP could play an important role in the regional O_3 formation. Therefore, HONO formation from atmospheric oxidation of NO_x should be taken into consideration for formulating O_3 control strategies in polluted areas.

METHODS

Smog chamber experiments

The experiments were conducted in a 3-m^3 collapsible Teflon environmental chamber at 25 ± 1 °C, which was irradiated by 63

black-light lamps with a central wavelength of 365 nm (Supplementary Fig. 5). Detailed information for the chamber was described in our previous studies[51,52]. The buffer gas (ultrapure N_2, ultrapure O_2 or synthetic air with the purity of ≥ 99.999 %) was introduced into the chamber at a flow rate of 70 L/min through a mass flow controller (Beijing Sevenstar Electronic Technology Co. Ltd., China). To achieve the target concentrations for each mixture, NO_x obtained from the standard gases (584 ppm NO in N_2 and 591 ppm NO_2 in N_2) and O_3 generated by an electrical discharge generator were directly introduced into the chamber with glass syringes. Additionally, water vapor was introduced into the chamber through bubbling a bubbler containing ultrapure water by 3 L/min N_2. Before each experiment, the chamber was flushed at least 3 times with the ultrapure N_2 to avoid possible interfering substances in the chamber.

NO_x (NO and NO_2) and O_3 were measured by the NO_x and O_3 analyzers (Model 42i and 49i, Thermo-fisher Scientific Inc, USA), respectively. HONO, HNO_3 and N_2O_5 were measured based on a wet chemical method[53]. In brief, they were absorbed by a stripping coil with 25 μM sodium carbonate solution. The gas and liquid flow rates were set to be 2 L min^{-1} and 0.25 mL min^{-1}, respectively. After sampling, NO_2^- and NO_3^- in the absorption solution were measured by an ion chromatography[54,55] (IC, WAYEAL IC6200, China). The wet chemical method for HONO and HNO_3 measurement has been systematically evaluated and widely used in the previous studies[11,53,56]. It should be mentioned that the measured NO_3^- in the absorption solution represented the sum of HNO_3 and N_2O_5 levels. Considering that N_2O_5 formation can be obviously suppressed when NO levels began to accumulate in the chamber, the measured NO_3^- in the absorption solution with the existence of excess NO should be attributed to HNO_3 which had been formed from hydrolysis of N_2O_5 on the chamber wall. N_2O_5 concentrations before introduction of NO were roughly calculated by subtracting HNO_3 concentration from the sum NO_3^- concentration in the absorption solution collected from the chamber.

WRF-Chem configuration

The WRF-Chem model (ver. 4.0.3)[57] was adopted to explore the relative contributions of various HONO sources to atmospheric HONO. Carbon Bond Mechanism version-Z (CBMZ) scheme[58] coupled with the 4-bin sectional Model for Simulating Aerosol Interactions and Chemistry (MOSAIC) scheme[59] were used as the gas and aerosol chemical mechanisms in the model, respectively. The anthropogenic emission data were obtained from the Multi-resolution Emission Inventory for China with base year of 2017 (MEIC-2017) with a resolution of 0.25° × 0.25° (http://www.meicmodel.org/)[60]. The biogenic emissions were estimated online by the Model of Emissions of Gases and Aerosols from Nature version 2.1 (MEGAN v2.1)[61].

The major HONO sources, including the direct emission, the heterogeneous reactions and the photo-enhanced reductions of NO_2 on aerosol and ground surfaces, and the photolysis of particulate nitrate, were incorporated into the emission module and MOSAIC chemical mechanism in WRF-Chem model, respectively. The new HONO sources identified by this study were added into MOSAIC chemical mechanism and CBMZ chemical mechanism, respectively. Other WRF-Chem configurations adopted in this study were listed in Supplementary Table 2. The simulations were performed from 1st to 22nd June 2017 with 7-day spin-up period on a domain covering the North China Plain (NCP), centered at 39.5 °N, 114.8 °E, with 9 km horizontal resolution, 223 × 202 grid cells, and 30 vertical levels from the ground level of 17 m to the maximum pressure of 50 hPa. For more details, see Supplementary Methods.

DATA AVAILABILITY

Raw data used in this study are archived at Research Center for Eco-environmental Sciences, Chinese Academy Sciences, and are available on request by contacting the corresponding authors (pfliu@rcees.ac.cn; yjmu@rcees.ac.cn).

Received: 29 June 2022; Accepted: 28 March 2023;
Published online: 11 April 2023

REFERENCES

1. Finlayson-Pitts, B. J. *Atmospheric Chemistry: Fundamentals and Experimental Techniques* (Wiley, 1986).
2. Xue, C. et al. HONO budget and its role in nitrate formation in the rural North China Plain. *Environ. Sci. Technol.* **54**, 11048–11057 (2020).
3. Kim, S. et al. The primary and recycling sources of OH during the NACHTT-2011 campaign: HONO as an important OH primary source in the wintertime. *J. Geophys. Res.: Atmos.* **119**, 6886–6896 (2014).
4. Lee, J. et al. Detailed budget analysis of HONO in central London reveals a missing daytime source. *Atmos. Chem. Phys.* **16**, 2747–2764 (2016).
5. Kleffmann, J. et al. Measured and simulated vertical profiles of nitrous acid-Part I: field measurements. *Atmos. Environ.* **37**, 2949–2955 (2003).
6. Su, H. et al. Nitrous acid (HONO) and its daytime sources at a rural site during the 2004 PRIDE-PRD experiment in China. *J. Geophys. Res.: Atmos.* **113**, D14312 (2008).
7. George, C., Strekowski, R., Kleffmann, J., Stemmler, K. & Ammann, M. Photo-enhanced uptake of gaseous NO_2 on solid organic compounds: a photochemical source of HONO? *Faraday Discuss* **130**, 195–210 (2005).
8. Stemmler, K., Ammann, M., Donders, C., Kleffmann, J. & George, C. Photosensitized reduction of nitrogen dioxide on humic acid as a source of nitrous acid. *Nature* **440**, 195–198 (2006).
9. Han, C., Yang, W., Wu, Q., Yang, H. & Xue, X. Heterogeneous photochemical conversion of NO_2 to HONO on the humic acid surface under simulated sunlight. *Environ. Sci. Technol.* **50**, 5017–5023 (2016).
10. Zhou, X. et al. Nitric acid photolysis on forest canopy surface as a source for tropospheric nitrous acid. *Nat. Geosci.* **4**, 440–443 (2011).
11. Laufs, S. & Kleffmann, J. Investigations on HONO formation from photolysis of adsorbed HNO_3 on quartz glass surfaces. *Phys. Chem. Chem. Phys.* **18**, 9616–9625 (2016).
12. Ye, C., Gao, H., Zhang, N. & Zhou, X. Photolysis of nitric acid and nitrate on natural and artificial surfaces. *Environ. Sci. Technol.* **50**, 3530–3536 (2016).
13. Bao, F., Li, M., Zhang, Y., Chen, C. & Zhao, J. Photochemical aging of Beijing urban $PM_{2.5}$: HONO production. *Environ. Sci. Technol.* **52**, 6309–6316 (2018).
14. Su, H. et al. Soil nitrite as a source of atmospheric HONO and OH radicals. *Science* **333**, 1616–1618 (2011).
15. Oswald, R. et al. HONO emissions from soil bacteria as a major source of atmospheric reactive nitrogen. *Science* **341**, 1233–1235 (2013).
16. VandenBoer, T. C. et al. Nocturnal loss and daytime source of nitrous acid through reactive uptake and displacement. *Nat. Geosci.* **8**, 55–60 (2015).
17. Donaldson, M. A., Bish, D. L. & Raff, J. D. Soil surface acidity plays a determining role in the atmospheric-terrestrial exchange of nitrous acid. *Proc. Natl. Acad. Sci. USA* **111**, 18472–18477 (2014).
18. Li, S., Matthews, J. & Sinha, A. Atmospheric hydroxyl radical production from electronically excited NO_2 and H_2O. *Science* **319**, 1657–1660 (2008).
19. Amedro, D., Parker, A. E., Schoemaecker, C. & Fittschen, C. Direct observation of OH radicals after 565 nm multi-photon excitation of NO_2 in the presence of H_2O. *Chem. Phys. Lett.* **513**, 12–16 (2011).
20. Bejan, I. et al. The photolysis of ortho-nitrophenols: a new gas phase source of HONO. *Phys. Chem. Chem. Phys.* **8**, 2028–2035 (2006).
21. Yang, W. et al. Photolysis of nitroaromatic compounds under sunlight: a possible daytime photochemical source of nitrous acid? *Environ. Sci. Technol. Lett.* **8**, 747–752 (2021).
22. Li, X. et al. Missing gas-phase source of HONO inferred from Zeppelin measurements in the troposphere. *Science* **344**, 292–296 (2014).
23. Liu, Y. et al. A comprehensive model test of the HONO sources constrained to field measurements at rural North China Plain. *Environ. Sci. Technol.* **53**, 3517–3525 (2019).
24. Wang, Y. et al. Agricultural fertilization aggravates air pollution by stimulating soil nitrous acid emissions at high soil moisture. *Environ. Sci. Technol.* **55**, 14556–14566 (2021).
25. Xing, L. et al. Wintertime secondary organic aerosol formation in Beijing–Tianjin–Hebei (BTH): contributions of HONO sources and heterogeneous reactions. *Atmos. Chem. Phys.* **19**, 2343–2359 (2019).

26. Neuman, J. A. et al. HONO emission and production determined from airborne measurements over the Southeast U.S. *J. Geophys. Res.-Atmos.* **121**, 9237–9250 (2016).
27. Ye, C. et al. Tropospheric HONO distribution and chemistry in the southeastern US. *Atmos. Chem. Phys.* **18**, 9107–9120 (2018).
28. Mollner, A. K. et al. Rate of gas phase association of hydroxyl radical and nitrogen dioxide. *Science* **330**, 646–649 (2010).
29. Atkinson, R. et al. Evaluated kinetic and photochemical data for atmospheric chemistry: volume I-gas phase reactions of O_x, HO_x, NO_x and SO_x species. *Atmos. Chem. Phys.* **4**, 1461–1738 (2004).
30. Finlayson-Pitts, B. J., Wingen, L. M., Sumner, A. L., Syomin, D. & Ramazan, K. A. The heterogeneous hydrolysis of NO_2 in laboratory systems and in outdoor and indoor atmospheres: An integrated mechanism. *Phys. Chem. Chem. Phys.* **5**, 223–242 (2003).
31. Pitts, J. N. Jr et al. An investigation of the dark formation of nitrous acid in environmental chambers. *Int. J. Chem. Kinet.* **16**, 919–939 (1984).
32. Zádor, J., Turányi, T., Wirtz, K. & Pilling, M. J. Measurement and investigation of chamber radical sources in the European Photoreactor (EUPHORE). *J. Atmos. Chem.* **55**, 147–166 (2006).
33. Rohrer, F. et al. Characterisation of the photolytic HONO-source in the atmosphere simulation chamber SAPHIR. *Atmos. Chem. Phys.* **5**, 2189–2201 (2005).
34. Gardner, E. P., Sperry, P. D. & Calvert, J. G. Primary quantum yields of NO_2 photodissociation. *J. Geophys. Res.: Atmos.* **92**, 6642–6652 (1987).
35. Schwantes, R. H. et al. *Advances in Atmospheric Chemistry*: Ch. 1, 1–93 (World Scientific, 2017).
36. Svensson, R. & Ljungström, E. A kinetic study of the decomposition of HNO_3 and its reaction with NO. *Int. J. Chem. Kinet.* **20**, 857–866 (1988).
37. Hauglustaine, D., Ridley, B., Solomon, S., Hess, P. & Madronich, S. HNO_3/NO_x ratio in the remote troposphere during MLOPEX 2: Evidence for nitric acid reduction on carbonaceous aerosols? *Geophys. Res. Lett.* **23**, 2609–2612 (1996).
38. Saliba, N., Yang, H. & Finlayson-Pitts, B. Reaction of gaseous nitric oxide with nitric acid on silica surfaces in the presence of water at room temperature. *J. Phys. Chem. A* **105**, 10339–10346 (2001).
39. Muñoz, M. S. & Rossi, M. Heterogeneous reactions of HNO_3 with flame soot generated under different combustion conditions. Reaction mechanism and kinetics. *Phys. Chem. Chem. Phys.* **4**, 5110–5118 (2002).
40. Li, X. et al. Abiotic degradation of field wheat straw as a notable source of atmospheric carbonyls in the North China Plain. *Sci. Total Environ.* **811**, 151366 (2022).
41. Peng, X., Wang, W., Xia, M., Chen, H. & Wang, T. An unexpected large continental source of reactive bromine and chlorine with significant impact on wintertime air quality. *Natl. Sci. Rev.* **8**, nwaa304 (2021).
42. Ye, C. et al. Particle-phase photoreactions of HULIS and TMIs establish a strong source of H_2O_2 and particulate sulfate in the winter North China Plain. *Environ. Sci. Technol.* **55**, 7818–7830 (2021).
43. Zhang, W. et al. Different HONO sources for three layers at the urban area of Beijing. *Environ. Sci.Technol.* **54**, 12870–12880 (2020).
44. Zhang, J., An, J., Qu, Y., Liu, X. & Chen, Y. Impacts of potential HONO sources on the concentrations of oxidants and secondary organic aerosols in the Beijing-Tianjin-Hebei region of China. *Sci. Total Environ.* **647**, 836–852 (2019).
45. Zhang, L. et al. Potential sources of nitrous acid (HONO) and their impacts on ozone: A WRF-Chem study in a polluted subtropical region. *J. Geophys. Res.: Atmos.* **121**, 3645–3662 (2016).
46. Qin, M. et al. An observational study of the HONO–NO_2 coupling at an urban site in Guangzhou City, South China. *Atmos. Environ.* **43**, 5731–5742 (2009).
47. Hofzumahaus, A. et al. Amplified trace gas removal in the troposphere. *Science* **324**, 1702–1704 (2009).
48. Liu, P. et al. Photochemical aging of atmospheric fine particles as a potential source for gas-phase hydrogen peroxide. *Environ. Sci. Technol.* **55**, 15063–15071 (2021).
49. Zhang, Y. et al. Photoinduced uptake and oxidation of SO_2 on Beijing urban $PM_{2.5}$. *Environ. Sci. Technol.* **54**, 14868–14876 (2020).
50. Corral Arroyo, P. et al. Particle-phase photosensitized radical production and aerosol aging. *Environ. Sci. Technol.* **52**, 7680–7688 (2018).
51. Song, M. et al. The influence of OH concentration on SOA formation from isoprene photooxidation. *Sci. Total Environ.* **650**, 951–957 (2019).
52. Song, M. et al. The influence of UV-light irradiation and stable Criegee intermediate scavengers on secondary organic aerosol formation from isoprene ozonolysis. *Atmos. Environ.* **191**, 116–125 (2018).
53. Xue, C. et al. Development of stripping coil-ion chromatograph method and intercomparison with CEAS and LOPAP to measure atmospheric HONO. *Sci. Total Environ.* **646**, 187–195 (2019).
54. Liu, P. et al. The possible contribution of the periodic emissions from farmers' activities in the North China Plain to atmospheric water-soluble ions in Beijing. *Atmos. Chem. Phys.* **16**, 10097–10109 (2016).
55. Liu, P. et al. Fine particle pH and its influencing factors during summer at Mt. Tai: Comparison between mountain and urban sites. *Atmos. Environ.* **261**, 118607 (2021).
56. Kleffmann, J., Benter, T. & Wiesen, P. Heterogeneous reaction of nitric acid with nitric oxide on glass surfaces under simulated atmospheric conditions. *J. Phys. Chem. A* **108**, 5793–5799 (2004).
57. Grell, G. A. et al. Fully coupled "online" chemistry within the WRF model. *Atmos. Environ.* **39**, 6957–6975 (2005).
58. Zaveri, R. A. & Peters, L. K. A new lumped structure photochemical mechanism for large-scale applications. *J. Geophys. Res.: Atmos.* **104**, 30387–30415 (1999).
59. Zaveri, R. A., Easter, R. C., Fast, J. D. & Peters, L. K. Model for simulating aerosol interactions and chemistry (MOSAIC). *J. Geophys. Res.: Atmos.* **113**, D13024 (2008).
60. Li, M. et al. Anthropogenic emission inventories in China: a review. *Natl. Sci. Rev* **4**, 834–866 (2017).
61. Guenther, A. et al. The Model of emissions ofgases and aerosols from nature version 2.1 (MEGAN2. 1): an extended and updated framework for modeling biogenic emissions. *Geosci. Model Dev.* **5**, 1471–1492 (2012).

ACKNOWLEDGEMENTS

The work was supported by the National Key Research and Development Program (2022YFC3701102) and the National Natural Science Foundation of China (91544211, 41727805, 21976108, 41905109).

AUTHOR CONTRIBUTIONS

Y.M. designed the study. P.L. and M.S. designed the chamber experiments. M.S. and J.M. carried out the chamber experiments. X.X.Z. and X.J.Z. performed model simulations. G.H. performed DFT calculation. M.S., P.L. and X.X.Z. draw the figures. S.T. and M.G. provided HONO observation data in Beijing. Y.M., P.L., S.M. and X.X.Z. analyzed the chamber data and wrote the paper with valuable inputs from all authors.

COMPETING INTERESTS

The authors declare no competing interests.

ADDITIONAL INFORMATION

Supplementary information The online version contains supplementary material available at https://doi.org/10.1038/s41612-023-00357-8.

Correspondence and requests for materials should be addressed to Pengfei Liu or Yujing Mu.

Reprints and permission information is available at http://www.nature.com/reprints

Publisher's note Springer Nature remains neutral with regard to jurisdictional claims in published maps and institutional affiliations.